Chinese Journal of Polymer Science Vol. 35, No. 8, (2017), 974–991

Chinese Journal of Polymer Science
© Chinese Chemical Society
Institute of Chemistry, CAS
Springer-Verlag Berlin Heidelberg 2017

Effect of Star-shaped Chain Architectures on the Polylactide Stereocomplex Crystallization Behaviors*

Ke-yu Zhou[a, b], Jian-bo Li[a**], Han-xuan Wang[b] and Jie Ren[a, b**]

[a] *Key Laboratory of Advanced Civil Engineering Materials of Ministry of Education, School of Materials Science and Engineering, Tongji University, Shanghai 200092, China*

[b] *Institute of Nano and Bio-Polymeric Materials, School of Material Science and Engineering, Tongji University, Shanghai 201804, China*

Abstract Linear and star-shaped polylactides (PLA) with similar molecular weights of each arm are synthesized *via* ring-opening polymerization of LA with 3-butyn-1-ol and pentaerythritol as initiators, respectively. By solution blending of equivalent mass of poly(L-lactic acid)s (PLLAs) and poly(D-lactic acid)s (PDLAs), perfect PLA stereocomplexes (scPLAs) are prepared and confirmed by WAXD and FTIR analysis. Effect of chain architectures on stereocomplex crystallization is investigated by studying the non-isothermal and isothermal crystallization of linear and star-shaped polylactide stereocomplexes. In dynamic DSC and POM test, star-shaped PLLA (4sPLLA)/PDLA and PLLA/star-shaped PDLA (4sPDLA) stereocomplexes reach rapid crystallization and higher crystallinity due to larger spherulite density of star-shaped chain and excellent chain mobility of linear chain. In isothermal crystallization test, much faster crystallization and less crystallization half-time is obtained with the increase of star-shaped chain. Meanwhile, 4sPLLA/PDLA and PLLA/4sPDLA are found to have the highest crystallinity, suggesting limitation of too much star-shaped chain for 4sPLLA/4sPDLA and restriction of linear chain in nucleation capacity for PLLA/PDLA. The results reveal that star-shaped chain has an important influence on the crystallization of scPLAs.

Keywords Polylactic acid; Stereocomplex; Linear; Star-shaped; Crystallization

INTRODUCTION

Polylactide (PLA) is one of the biodegradable plastics with good biological compatibility and excellent mechanical properties, attracting considerable attention in recent years. Polylactides is widely used in packaging, textile, construction, electronic and biomedical equipment fields[1–5]. However, under conventional processing conditions, polylactides has low crystallinity and poor heat resistance due to its slow crystallization rate, which limits its industrial and commodity applications[6, 7]. Therefore, improving the heat resistance of polylactides is an essential issue to enlarge the potential use range of PLA[7, 8].

There are many factors that affect the heat resistance of PLA, including the chemical structure of PLA, molecular weight, molding conditions[9–11]. Up to now, many routes are exploited to improve the heat resistance of PLA, such as additives, like nucleating agents[12–16], plasticizers[17–19], and nanoparticles[20], which can increase the chain mobility and the number of crystallization sites, thus accelerating the crystallization and

* This work was financially supported by the National High-Tech R&D Program of China (No. 2013AA032202), the National Natural Science Foundation of China (No. 51203118), the Fundamental Research Funds for the Central Universities and the Open Funds for Characterization of Tongji University.

** Corresponding authors: Jian-bo Li (李建波), E-mail: lijianbo@tongji.edu.cn
Jie Ren (任杰), E-mail: renjie6598@163.com

Received December 19, 2016; Revised January 16, 2017; Accepted January 23, 2017
doi: 10.1007/s10118-017-1935-4

increasing the T_m of PLA. Other approaches, like blending[21], or copolymerization with other polymers[20], cross-linking[22], and adjusting technological conditions, can also have an effect on the heat resistance of PLA.

Another effective method to enhance heat resistance of PLA is preparation of stereocomplex (sc) crystals which can be obtained by mixing two enantiomers of PLA, *i.e.*, PLLA and PDLA. Since first reported by Ikada *et al.*[23], stereocomplex of PLA has been extensively studied due to its excellent properties caused by its specific crystal structure. When equimolar PLLA and PDLA are mixed, they can cocrystallize and form stereocomplex, which has a 3_1 helical conformation, different from the 10_3 helical one formed by homopolymer crystals[24]. The enantiomeric chains in sc crystallites pack more tightly than those of the homopolymer crystals through the intermolecular hydrogen bonding interactions between methyl and carbonyl groups[25]. The peculiar structural feature renders scPLA with many improved physical properties such as superior mechanical strength and better resistance to thermal, solvent and hydrolytic degradation[26, 27]. The melting temperature (T_m) of scPLA ($T_m \approx$ 230 °C) is approximately 50 °C higher than that of homochiral PLA crystals.

It is reported that the stereocomplexation crystallization of PLA will be largely influenced by various factors, including molar mass, blending ratio, preparation routes, optical purity and processing conditions[28–32]. It has been well recognized that molecular weight is a critical factor for sc crystallization in PLLA/PDLA blends. Generally speaking, low molecular weight and equimolar ratio are favorable for stereocomplexation crystallization[29]. In addition, branched architecture is also a hot spot for the research on PLA stereocomplexes[33]. Melting point, melting enthalpy and hydrolytic degradation rate would be affected by the stereocomplexation of star-shaped D-LA oligomers and PLLA[34]. Shao *et al.*[35] investigated the influence of molecular weight, structure and constituents on 3PLLA/PDLA and 3PLLA/3PDLA stereocomplexes. Biela *et al.*[36] found stereocomplexes were easy to form when PLLA with 13 or more branches was blended with its enantiomers. Branched architectures[37], 3D core structure[38, 39], and dendrimer[40] would also promote the formation of stereocomplex. Sakamoto *et al.*[41] revealed that crystallization was delayed during heating from melt-quenched specimen by the branching effects. Stereocomplexes consisting of copolymers like PEG-PLA[42–45] and star-shaped PLLA-*b*-PDLA[46–48] also presented special performance. In general, star-shaped polymers could exhibit many different properties as compared to linear ones, such as smaller hydrodynamic radius, lower melt viscosity and special crystallization behavior. Therefore, many unique sc crystallization behavior may appear when scPLA is developed from linear/linear, linear/branched, branched/branched blends. For example, Bao *et al.*[49] discovered that comblike/comblike blends crystallized faster and preferred sc crystallization compared with linear/linear and linear/comblike blends for PLA with high molecular weight due to the existence of multiple branch points. But it has not been systematically studied whether the star-shaped PLA with one branch point possesses the same or peculiar crystallization behavior.

In this work, we focus on the effect of star-shaped chain architectures on crystallization behaviors of scPLA. Linear and star-shaped PLAs with similar molecular weights of each arm were synthesized *via* ring-opening polymerization of LA using 3-butyn-1-ol and pentaerythritol as initiators, respectively. The molecular structure, non-isothermal and isothermal crystallization kinetics of linear/linear racemic blends were systematically investigated and compared with those of linear/star-shaped and star-shaped/star-shaped blends by nuclear magnetic resonance (NMR), Fourier transform infrared spectroscopy (FTIR), wide-angle X-ray diffraction (WAXD), differential scanning calorimetry (DSC), and polarizing optical microscopy (POM). It was found that linear/star-shaped blends behaved better in crystallization than linear/linear and star-shaped/star-shaped blends and the mechanism was discussed and proposed.

EXPERIMENTAL

Materials

L-lactide (L-LA) and D-lactide (D-LA) (99.3%, Jinan Daigang Biomaterial Co., Ltd.) were purified by recrystallization from toluene three times and dried in vacuum at room temperature. 3-Butyn-1-ol (Adamas) was distilled under reduced pressure before use. Pentaerythritol (Aldrich) was dried at 60 °C in vacuo for 24 h before use. Tin 2-ethylhexanoate ($Sn(Oct)_2$, Aldrich) was distilled under reduced pressure before use. Other reagents

were used as received.

Synthesis of Linear PLLA, Linear PDLA, Star-shaped PLLA (4sPLLA) and Star-shaped PDLA (4sPDLA)

Linear PLLA, linear PDLA, 4sPLLA, 4sPDLA were synthesized *via* ring-opening polymerization (ROP) of lactide using 3-butyn-1-ol or pentaerythritol as initiators and $Sn(Oct)_2$ as catalyst, according to a published method[50]. A typical polymerization procedure for linear PLLA with an expected M_n of 1.0×10^4 g·mol^{-1} is described as follows. Briefly, L-LA (10.10 g, 70.0 mmol), 3-butyn-1-ol (0.07 g, 1.0 mmol) and $Sn(Oct)_2$ catalyst (0.07 mmol) and a magnetic stirrer were added to a 25 mL round-bottom flask. The flask was degassed with three freeze-evacuate-thaw cycles. Then the flask was kept in an oil bath at 115 °C under argon atmosphere with magnetic stirring for 24 h. After reaction, the crude polymer was dissolved in chloroform and precipitated three times in cold methanol. The purified PLLA was dried in a vacuum oven at room temperature until a constant weight was reached. The synthesis process of linear PDLA, 4sPLLA and 4sPDLA were similar to the above, in addition to the initiator of 4sPLLA and 4sPDLA were pentaerythritol and their feeding ratio were calculated at 1.0×10^4 g·mol^{-1} per arm.

Preparation of PLA Stereocomplexes

The stereocomplexes of PLA were obtained *via* solution blending before film casting. The blend films used for physical measurements were prepared with the method described in the literature[29]. Firstly, equivalent mass of PLLA and PDLA with linear or star-shaped topology were separately dissolved in chloroform (10 mg·mL^{-1}) at room temperature. Then the solutions of PLLA and PDLA were mixed and stirred rigorously under the same temperature for 3 h. After that, the blend solution was cast onto a Petri dish, and the solvent was allowed to evaporate at room temperature for 24 h. Then the film was dried in vacuum at 60 °C to remove the residue solvent for 48 h prior to physical measurements. The linear PLLA/linear PDLA, linear PLLA/star-shaped PDLA, star-shaped PLLA/linear PDLA and star-shaped PLLA/star-shaped PDLA blends are denoted as PLLA/PDLA, PLLA/4sPDLA, 4sPLLA/PDLA, 4sPLLA/4sPDLA, respectively.

Characterization and Testing

Nuclear magnetic resonance (NMR)

^{1}H-NMR spectra of polymers (PLLA, PDLA, 4sPLLA, 4sPDLA) were recorded on a Bruker DMX-500 NMR spectrometer using $CDCl_3$ as the solvent. The chemical shifts were reported with respect to the solvent signal.

Gel permeation chromatography (GPC)

The average molecular weight and polydispersity of polymers (PLLA, PDLA, 4sPLLA, 4sPDLA) were determined using a gel permeation chromatograph instrument equipped with a Waters 150C separations module and a Waters differential refractometer. The PLA samples were dissolved in DMF at a concentration of 1.0–2.0 mg·mL^{-1}. The measurements were conducted using DMF to elute through two Waters Styragel HT columns and a linear column at 1.0 mL·min^{-1} at 30 °C. The molecular weights were calculated against polystyrene standards.

Fourier transform infrared (FTIR)

FTIR spectra of polymers (PLLA, 4sPLLA, PLLA/PDLA, 4sPLLA/PDLA, PLLA/4sPDLA, 4sPLLA/4sPDLA) were recorded by an EQUINOXSS /HYPERION2000 FTIR spectrometer (Bruker, Germany).

Wide angle X-ray diffraction (WAXD)

The WAXD patterns of polymers (PLLA, 4sPLLA, PLLA/PDLA, 4sPLLA/PDLA, PLLA/4sPDLA, 4sPLLA/4sPDLA) were recorded with a Rigaku D/max 2500 X-ray powder diffractometer using Cu Kα radiation (λ = 0.154 nm), which was operated at 50 kV and 250 mA, in a range of 2θ = 5° to 40° at a scan speed of 5 (°)·min^{-1}.

Differential scanning calorimetry (DSC)

DSC analysis of polymers (PLLA, 4sPLLA, PLLA/PDLA, 4sPLLA/PDLA, PLLA/4sPDLA, 4sPLLA/4sPDLA) was carried on a DSC-Q100 thermal analyzer under a nitrogen atmosphere to study the thermal behaviors,

including the isothermal and non-isothermal crystallization as well as the melting behavior. Samples were first heated from 20 °C to 260 °C at a rate of 10 K·min^{-1} to record the melting behaviors. For non-isothermal crystallization, samples were first heated from 20 °C to 260 °C and held for 3 min to eliminate the thermal history, then cooled to 20 °C and finally reheated to 260 °C to examine the crystallization and melting behaviors. Both the cooling and heating rates were 10 K·min^{-1}. For isothermal crystallization, samples were first heated to 260 °C and held for 3 min to erase the thermal history at a rate of 10 K·min^{-1}, followed by cooling to the desired crystallization temperatures (T_c = 120, 130 and 140 °C) at a cooling rate of 40 K·min^{-1} and held at this temperature until the completion of crystallization. The crystallinity of PLA homochiral (hc) and scPLA (sc) were calculated from melting enthalpy of PLA and scPLA based on Eqs. (1) and (2), respectively:

$$X_{c(hc)} = \Delta H_{m(hc)} / \Delta H^0_{m(hc)} \times 100\% \quad (1)$$

$$X_{c(sc)} = \Delta H_{m(sc)} / \Delta H^0_{m(sc)} \times 100\% \quad (2)$$

where $\Delta H^0_{m(hc)}$ is 93 J·g^{-1}[51] and $\Delta H^0_{m(sc)}$ is 142 J·g^{-1}[52] for the theoretical melting enthalpy of 100% homocrystallites and 100% stereocomplex crystallites, respectively.

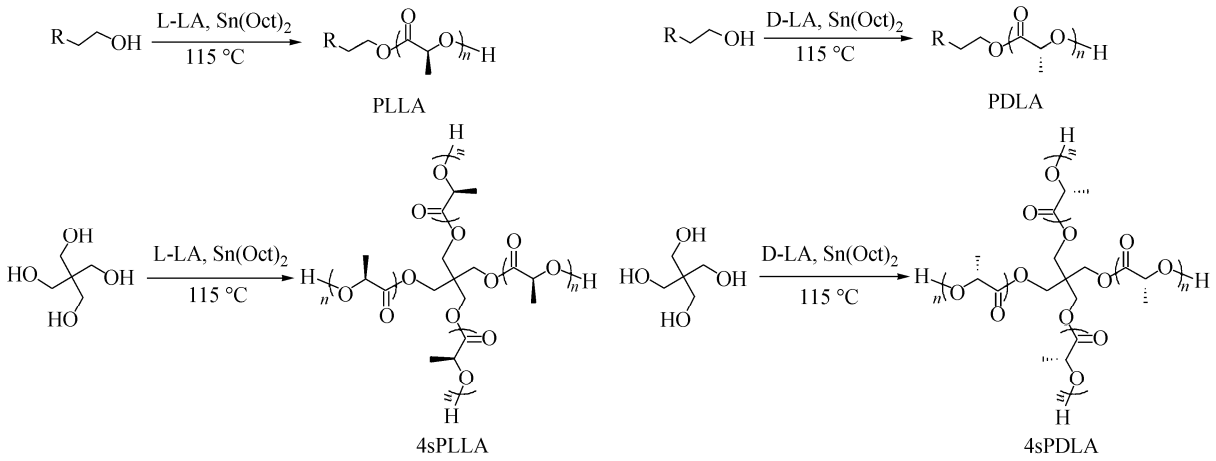
Polarized optical microscopy (POM)

The nucleation and crystalline morphology of polymers (PLLA/PDLA, 4sPLLA/PDLA, PLLA/4sPDLA, 4sPLLA/4sPDLA) were investigated using a polarized optical microscope (Germany LEICA DMLP) in combination with a Linkam THMS600 hot stage. For non-isothermal crystallization, samples squeezed between two glass slides were first melted at 260 °C to compress into films and held at 260 °C for 3 min to destroy thermal history, and then quickly cooled to room temperature at a rate of 10 K·min^{-1}. For isothermal crystallization, films were held at 260 °C for 3 min, then quickly cooled to the desired crystallization temperatures (T_c = 120, 130 and 140 °C). The morphologies of the growing crystals were monitored by taking photomicrographs at an appropriate time interval.

RESULTS AND DISCUSSION

Synthesis and Characterization of PLLAs and PDLAs

Linear PLLA, linear PDLA, 4sPLLA, 4sPDLA with the same M_w of each arm were synthesized *via* the ROP of lactides with 3-butyn-1-ol, and pentaerythritol as initiators, respectively (Scheme 1). The chemical structure of PLLAs was characterized by ^{1}H-NMR. Resonance peaks in the ^{1}H-NMR spectrum were assigned according to the literature[53]. As shown in Fig. 1, the typical signals of the methane and methyl protons of PLAs can be observed at 5.10 (peak a) and 1.58 (peak b), respectively, which indicates the successful synthesis of PLLAs and PDLAs.



Scheme 1 Synthesis of PLLA, PDLA, 4sPLLA and 4sPDLA

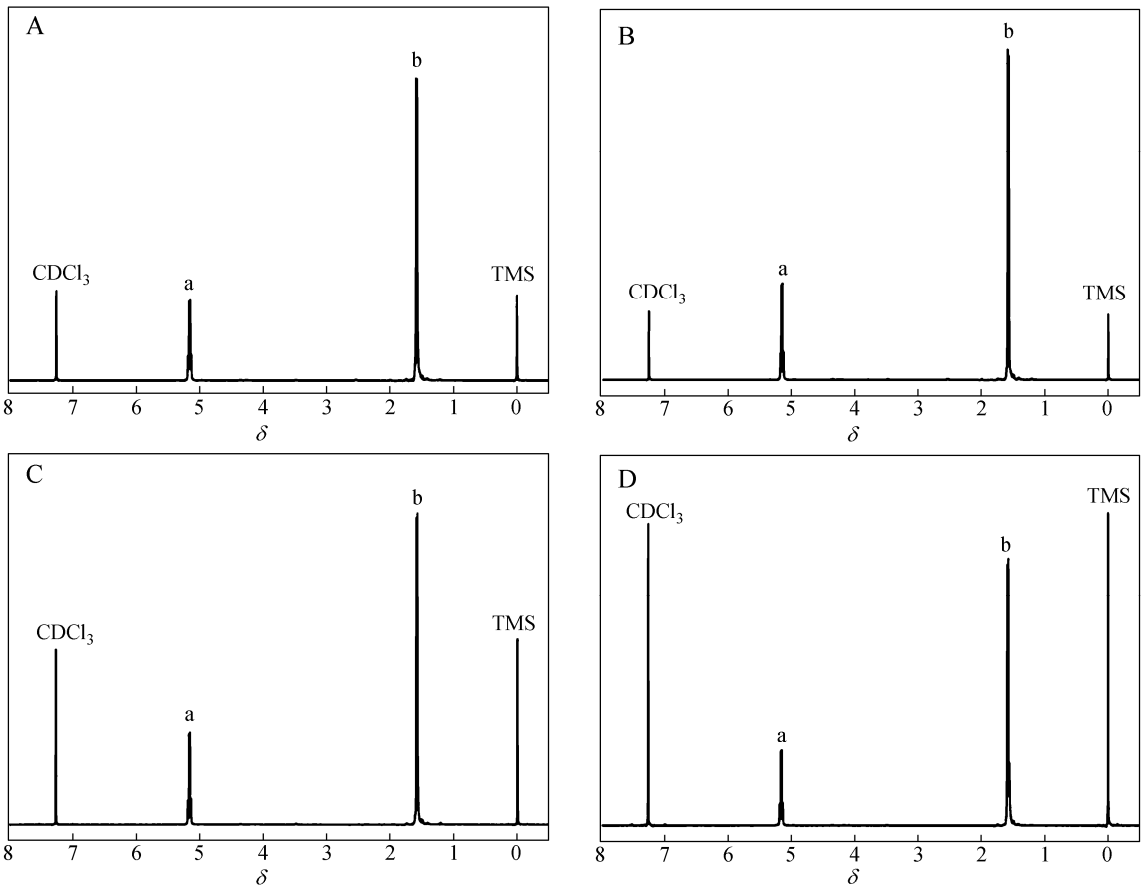


Fig. 1 ^{1}H-NMR spectra of (A) linear PLLA, (B) linear PDLA, (C) 4sPLLA and (D) 4sPDLA

The GPC traces of PLLA, PDLA, 4sPLLA, 4sPDLA and molecular weight achieved are shown in Fig. 2. The results of M_w were as expected and the monomodal traces of PLAs suggest that there are no mixture of star-shaped and linear polymers, further confirming the successful synthesis of the above polymers.

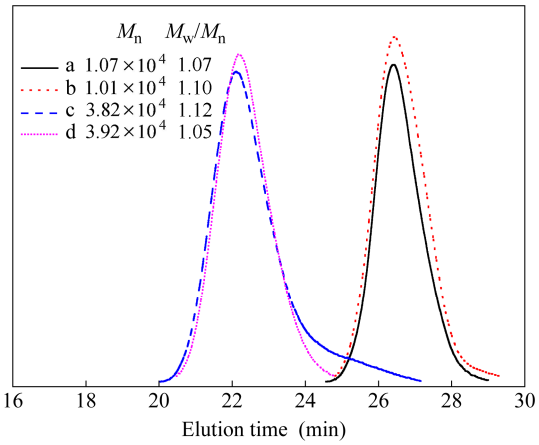


Fig. 2 GPC traces of (a) linear PLLA, (b) linear PDLA, (c) 4sPLLA and (d) 4sPDLA

Preparation and Characterization of PLA Stereocomplexes

Crystalline structures of PLLA, 4sPLLA, PLLA/PDLA, 4sPLLA/4sPDLA, 4sPLLA/PDLA, PLLA/4sPDLA were characterized by WAXD and FTIR spectral analysis[54]. Figure 3 shows the WAXD diffraction patterns of PLLA and 4sPLLA at 2θ = 14.6°, 16.5°, 18.9° and 22.6°, which can be attributed to the homocrystallites of PLLA and 4sPLLA, while PLLA/PDLA, 4sPLLA/4sPDLA, 4sPLLA/PDLA and PLLA/4sPDLA samples present prominent diffraction peaks at about 12°, 20.7° and 24°, corresponding to the characteristic diffraction peaks of sc crystallites. Besides, no characteristic reflection of hc crystallites are observed in sc crystallites, proving the formation of perfect stereocomplex crystallites without any homocrystallites.

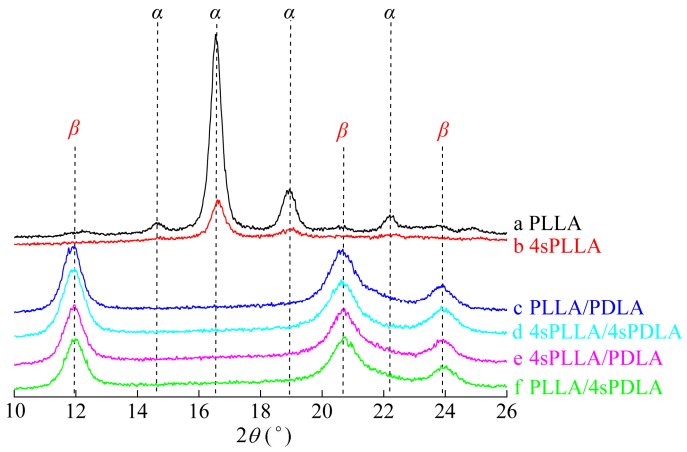


Fig. 3 WAXD patterns of (a) PLLA, (b) 4sPLLA, (c) PLLA/PDLA, (d) 4sPLLA/4sPDLA, (e) 4sPLLA/PDLA and (f) PLLA/4sPDLA

As has been reported, PLA stereocomplex formation is resulted from the hydrogen bonding between PLLA and PDLA, which can be verified by FTIR spectral measurements. Figures 4(a)–4(c) show typical IR spectra of hc and sc samples in the wavenumber regions of 935–885 cm^{-1}, 1800–1700 cm^{-1}, 3040–2920 cm^{-1}, respectively. Compared with the band of hc crystallites with the 10_3 conformation at 921 cm^{-1}, PLLA/PDLA, 4sPLLA/4sPDLA, 4sPLLA/PDLA and PLLA/4sPDLA samples show the characteristic band of sc crystallites at 908 cm^{-1}, associated with the 3_1 helical conformation in the sc crystalline phase. In addition, the formation of stereocomplex would also lead to a small shift to lower wavenumber in the C=O (1756 cm^{-1} to 1745 cm^{-1}) and C−H (2997 cm^{-1} to 2993 cm^{-1}, 2947 cm^{-1} to 2943 cm^{-1}) stretching regions corresponding to the formation of hydrogen bonding between methyl and carbonyl groups in the PLA stereocomplexes. All of the WAXD and FTIR spectral data confirm the perfect PLA stereocomplex formation.

Non-isothermal Crystallization

Non-isothermal crystallization behaviors of hc and sc samples were examined through DSC characterization. Samples were first melted at 260 °C for 3 min to eliminate the thermal history, then cooled to 20 °C and subsequently reheated to 260 °C at a rate of 10 $K \cdot min^{-1}$ to observe the crystallization and melting behaviors. Heating, cooling and reheating cycle are shown in Figs. 5(a), 5(b) and 5(c), respectively. As we can see, the endothermic and exothermic peaks of PLLA were larger than those of 4sPLLA, indicating larger crystallinity of PLLA than 4sPLLA. Compared with PLLA, 4sPLLA presented a slight cold crystallization peak in the second heating cycle, illustrating that 4sPLLA crystallized slower than PLLA. The result may be due to the negative effect of star-shaped structure on PLA crystallization; in other words, star-shaped structure disrupted the crystallization of PLA. As for PLA stereocomplexes, PLLA/PDLA and 4sPLLA/4sPDLA revealed a small exothermic peak in the cooling and second heating cycle, while 4sPLLA/PDLA and PLLA/4sPDLA showed larger exothermic peak in the cooling cycle and did not reveal any crystallization peak in the subsequent heating cycle, which indicated faster crystallization speed of 4sPLLA/PDLA and PLLA/4sPDLA than that of PLLA/PDLA and 4sPLLA/4sPDLA.

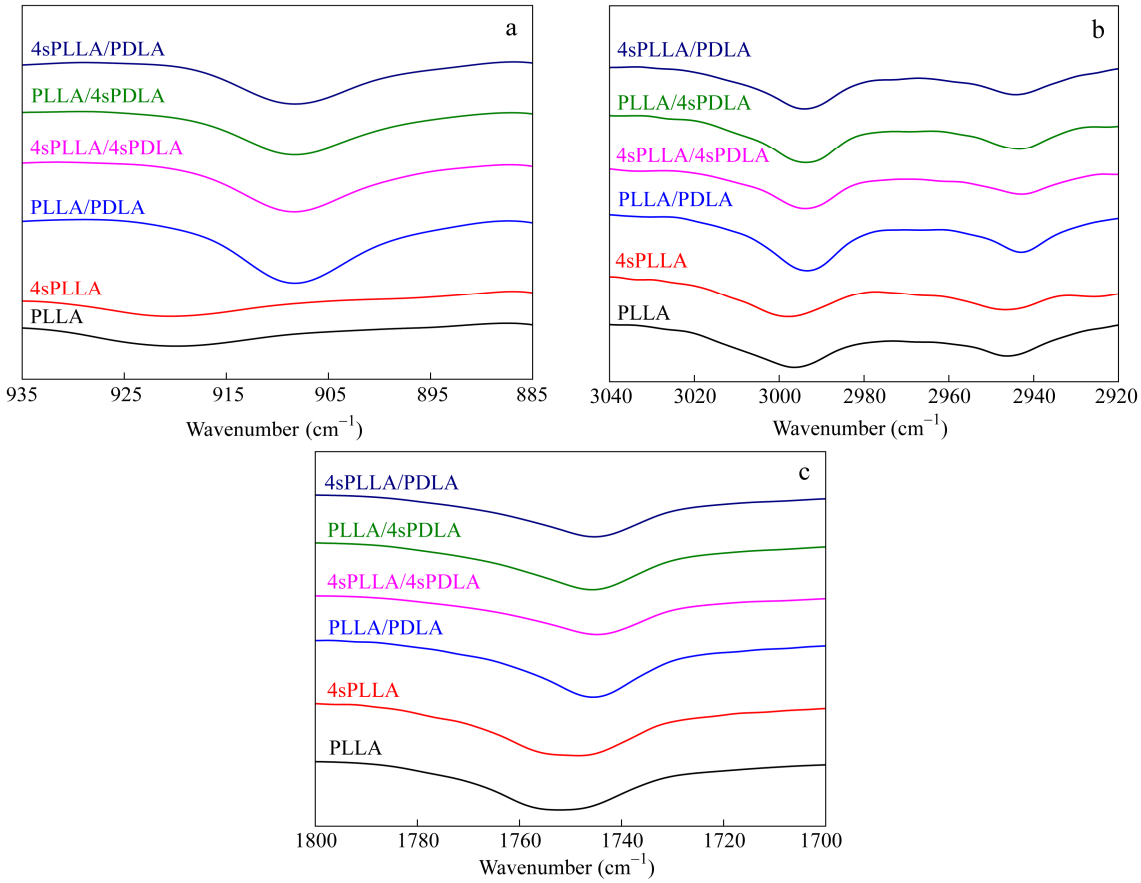


Fig. 4 IR spectra of various hc and sc samples in the range of (a) 935–885 cm^{-1}, (b) 3040–2920 cm^{-1}, (c) 1800–1700 cm^{-1}

Thermal properties of hc and sc crystallites obtained from Fig. 5 are summarized in Table 1. As we can see from the first heating cycle, the melting temperature (T_{m1}) of sc samples were 65–71 °C higher than the hc samples because of the hydrogen bonding interaction in sc samples. Besides, the T_{m1} of hc samples were similar while the T_{m1} of sc samples showed a slight difference. PLLA/PDLA showed the highest T_{m1} of 240.09 °C, nearly 9 °C higher than the lowest T_{m1} of 4sPLLA/4sPDLA due to the effect of steric hindrance in sc crystallites. The degree of crystallinity (X_{c1}) of linear samples also presented higher value than that of star-shaped samples. The X_{c1} of PLLA was twice that of 4sPLLA, and linear sc samples had more crystallites than star-shaped sc samples, which resulted in higher crystallization of the linear samples as influenced by the steric hindrance as well. 4sPLLA/4sPDLA had the lowest T_{m1} and X_{c1} as it was prepared *via* solution blending of star-shaped PLLA and star-shaped PDLA, which was affected more seriously than 4sPLLA/PDLA and PLLA/4sPDLA.

In the cooling cycle, the crystallization temperature (T_c) of PLLA was higher than that of 4sPLLA, which may be caused by the limitation of crystallization of star-shaped morphology. On the contrary, the higher T_c of star-shaped sc samples can be attributed to the faster crystallization kinetics of star-shaped structure. As we know, crystallization is the combination result of nucleation and growth. For 4sPLLA/PDLA and PLLA/4sPDLA, the less mobile chain segment caused by the chain tangles of star-shaped PLA would facilitate the presence of nucleus in the melt at high temperature while the chain segment of linear PLA was still free to move and growth was not restricted, thus the crystallization process was promoted. Compared to 4sPLLA/PDLA and PLLA/4sPDLA, 4sPLLA/4sPDLA was composed of two kinds of star-shaped PLA, leading to the promotion of nucleus and inhibition of growth at high temperature. In contrast, PLLA/PDLA had better growth ability and poorer nucleation capacity. As a result of the synthetic effect of nucleation and growth, the T_c of 4sPLLA/PDLA (PLLA/4sPDLA), 4sPLLA/4sPDLA, PLLA/PDLA decreased in turn.

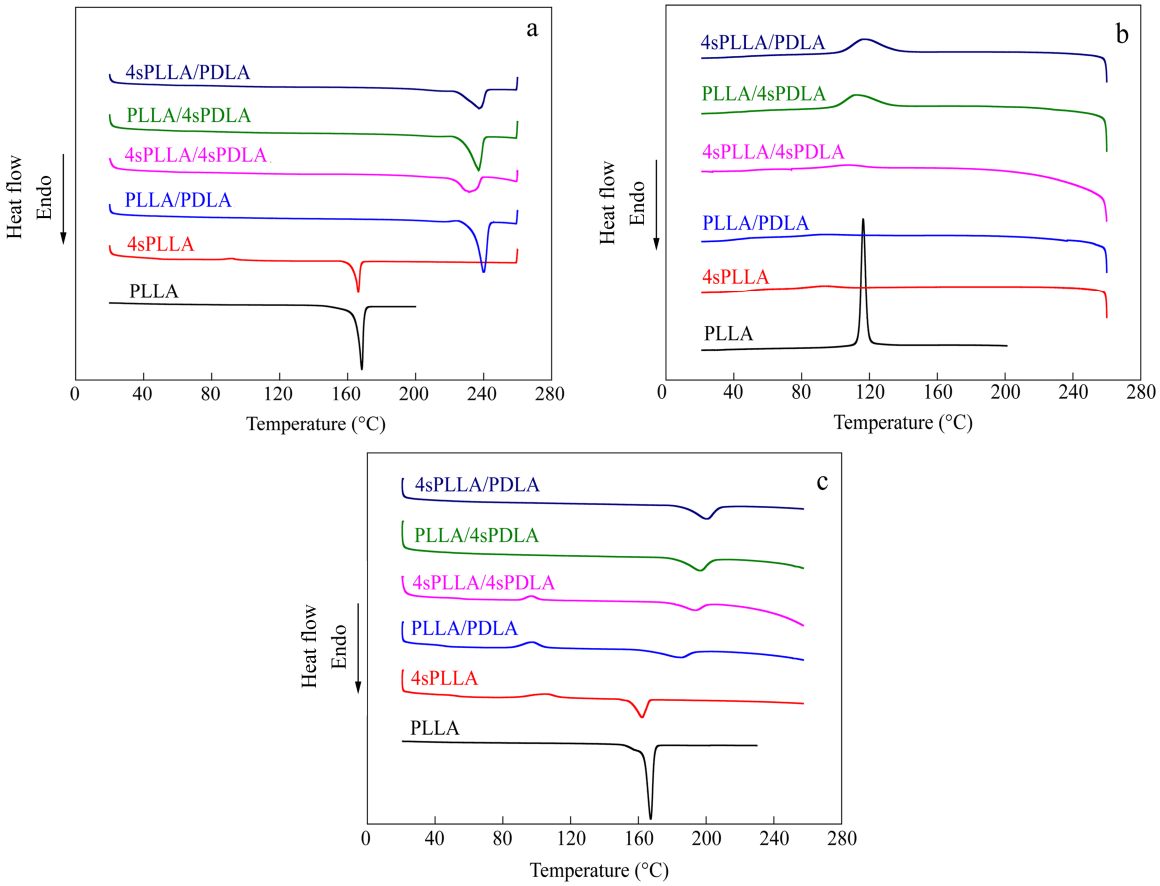


Fig. 5 DSC thermograms of hc and sc crystallites in dynamic mode at 10 K·min^{-1}: (a) first heating cycle, (b) cooling cycle and (c) second heating cycle

Table 1 Thermal properties of hc and sc crystallites in dynamic mode at 10 K·min^{-1}

Sample	First heating cycle			Cooling cycle	Second heating cycle			
	T_{m1} (°C)	X_{c1} (%)	ΔT_{m1} (°C)	T_c (°C)	T_{c2} (°C)	T_{m2} (°C)	X_{c2} (%)	ΔT_{m2} (°C)
PLLA	168.31	77.4	–	117.64	–	167.25	76.7	1.06
4sPLLA	166.19	35.4	–	93.33	105.50	162.22	34.7	3.97
PLLA/PDLA	240.09	72.1	71.78	92.89	97.59	185.11	21.2	54.98
4sPLLA/4sPDLA	231.57	38.0	65.38	107.19	108.00	193.17	15.0	38.40
PLLA/4sPDLA	237.15	58.3	68.84	111.91	–	196.47	28.2	40.68
4sPLLA/PDLA	237.59	41.3	71.40	116.42	–	200.21	30.2	37.38

T_{m1}, T_{m2} represent melting point; X_{c1}, X_{c2} represent crystallinity; T_c represents crystallization temperature; T_{c2} represents cold crystallization temperature; ΔT_{m1} represents the difference of melting point between hc and sc crystallites; ΔT_{m2} represents the difference of melting point between the first heating cycle and the second heating cycle.

In the second heating cycle, a small cold crystallization exothermic peak for 4sPLLA at 105.50 °C and finally less than half of the crystallinity of PLLA gave the point that star-shaped structure hindered the crystallization process of hcPLA. On the other hand, PLLA/4sPDLA and 4sPLLA/PDLA presented better performance in the reheating cycle since they had no cold crystallization peak, the highest T_{m2} and the largest X_{c2} among the four scPLAs, as a result of the fastest crystallization in the cooling cycle. It is worth noting that the melting enthalpy was used to estimate the crystallinity, containing crystallization in the cooling process and cold crystallization in the reheating process. Although 4sPLLA/4sPDLA crystallized faster than PLLA/PDLA in the

cooling cycle, it required higher temperature to loosen the tighter tangle between the star-shaped chain, which could be proved by the higher cold crystallization temperature (T_{c2}), leading to slower cold crystallization rate and smaller crystallinity (X_{c2}).

Comparing the first heating cycle with the second heating cycle, the melting point and crystallinity of hcPLA changed little, while scPLA showed a large difference due to the incomplete crystallization in dynamic mode at 10 K·min^{-1}. In the first heating cycle, PLLA/PDLA had higher melting point than 4sPLLA/4sPDLA, while in the second heating cycle an opposite result occurred. This may be caused by thicker lamellae of 4sPLLA/4sPDLA because of the higher crystallization temperature and its tighter tangled chain which needed higher temperature to obtain sufficient mobility.

The non-isothermal crystallization behaviors of sc samples were observed by polarized optical microscopy. Thermal history of thin films compressed between two glass slides was removed by heating at 260 °C for 3 min and micrographs were obtained as the temperature was cooled to 20 °C at a rate of 10 K·min^{-1}. The micrographs at the temperature of 150, 140, 130 and 120 °C are presented in Fig. 6. As we can see, small spherulite crystallites began to appear at 150 °C for star-shaped sc samples and continued to increase at lower temperature. Meanwhile, linear PLLA/PDLA sc sample did not crystallize at 150 °C until the temperature decreased to 130 °C. The faster crystallization of star-shaped stereocomplex was in agreement with the dynamic DSC measurement and higher spherulite density proved the findings that star-shaped structure would promote the nucleation process.

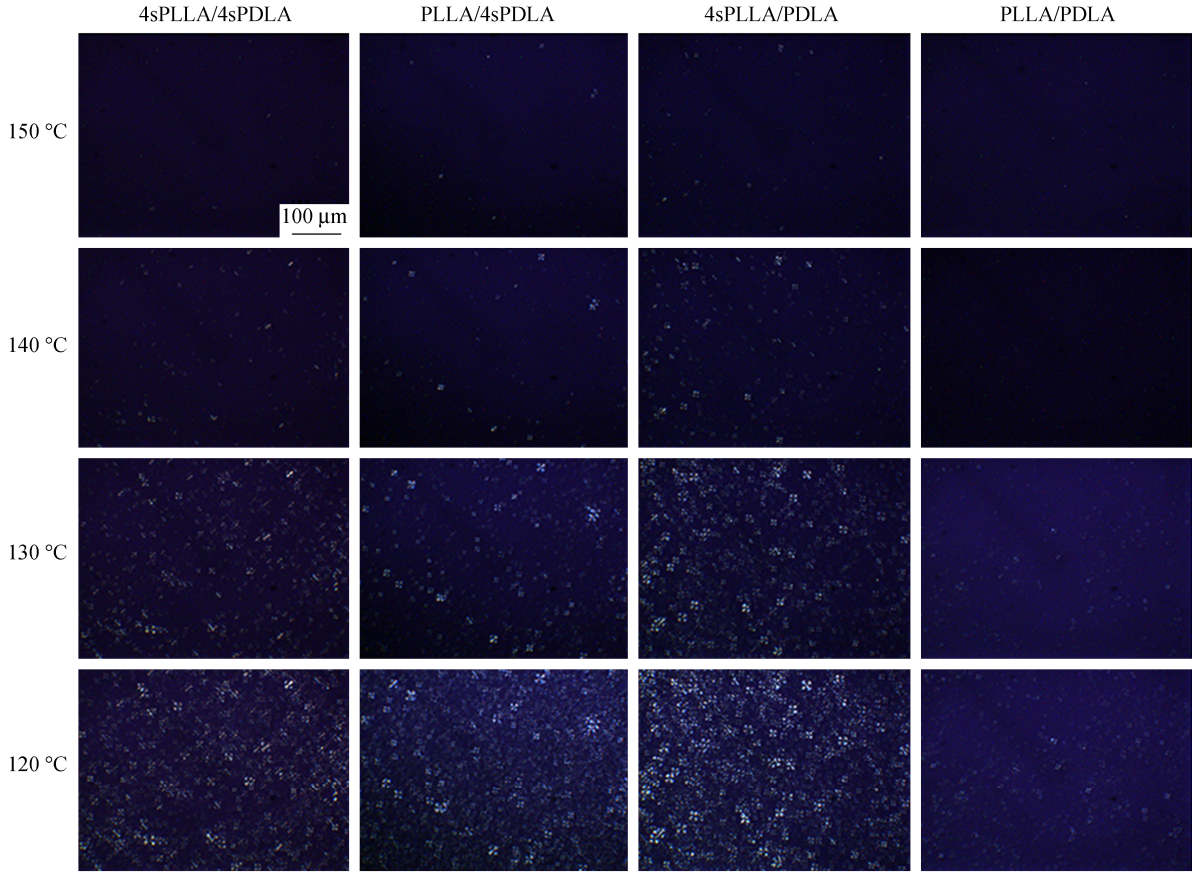


Fig. 6 POM images during non-isothermal crystallization for 4sPLLA/4sPDLA, PLLA/4sPDLA, 4sPLLA/PDLA and PLLA/PDLA (All the scale bars are the same.)

Isothermal Crystallization

To further reveal the effect of chain structure on the crystallization of scPLA, the isothermal crystallization behaviors of sc samples were investigated between 120 and 140 °C, as beyond the temperature range in which crystallization was either too fast or too little to observe. The four types of scPLA samples were melted at 260 °C for 3 min to destroy the thermal history, then cooled to the isothermal crystallization temperature (T_{iso}) as soon as possible and kept at this temperature until crystallization was complete. Heat flow versus time at different T_{iso} is plotted to reveal the crystallization of these scPLAs with time going on in Fig. 7. In Fig. 7(a), PLLA/PDLA had a sharper crystallization peak than 4sPLLA/4sPDLA, although they completely crystallized for almost the same time. PLLA/4sPDLA and 4sPLLA/PDLA had the sharpest and narrowest peak, indicating their fastest crystallization. In Fig. 7(b), the crystallization peaks of the three star-shaped scPLAs widened to similar extent while the peak of linear scPLA tailed to longer crystallization time, which means star-shaped scPLAs were affected less than linear scPLA when the T_{iso} was raised from 120 °C to 130 °C. As T_{iso} continued to increase from 130 °C to 140 °C, the peaks of PLLA/4sPDLA and 4sPLLA/PDLA widened more than that of 4sPLLA/4sPDLA. Meanwhile, the crystallization peak of PLLA/PDLA was almost invisible.

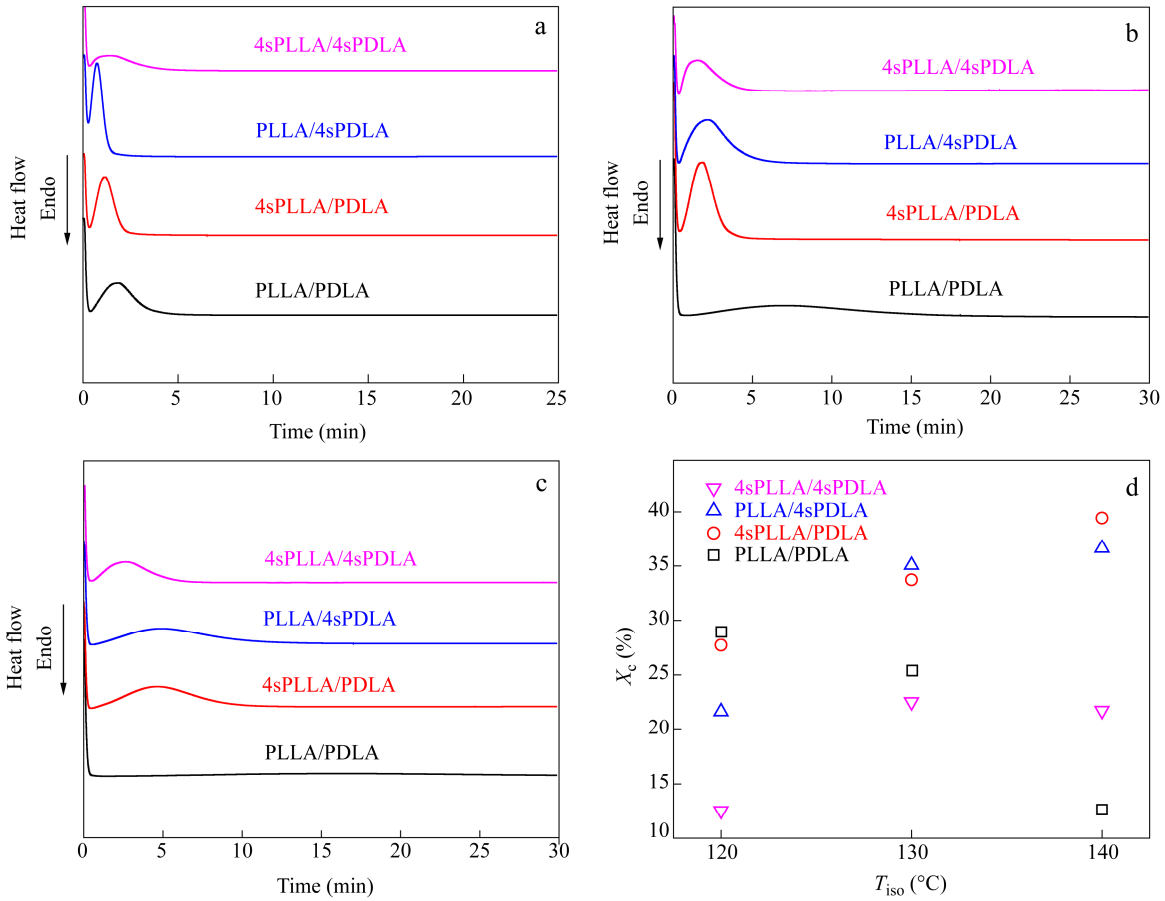


Fig. 7 DSC thermograms of sc specimen by isothermally annealing at (a) 120 °C, (b) 130 °C and (c) 140 °C; (d) Crystallinity achieved at these temperatures

According to Figs. 7(a)–7(c), a speculation may be drawn that nucleation and growth of crystals have temperature and structure sensitivity. As a result, different crystallization occurred for four scPLA samples with different T_{iso}. At 120 °C, 4sPLLA/4sPDLA had the best nucleation efficiency due to the tangled star-shaped chain and the poorest growth because of the terrible star-shaped chain mobility, while PLLA/PDLA was on the

contrary condition for its linear chain. Therefore, 4sPLLA/4sPDLA displayed similar crystallization speed as PLLA/PDLA. For 4sPLLA/PDLA and PLLA/4sPDLA, the mixture of star-shaped and linear chain ensured excellent nucleation capability and growth ability, leading to the fastest crystallization. When T_{iso} was raised to 130 °C, the growth ability of crystals improved and nucleation capability became more significant. As a consequence, similar crystallization tendency occurred on the star-shaped scPLAs while PLLA/PDLA exhibited more crystallization time. Finally, as T_{iso} went to 140 °C, higher temperature endowed star-shaped and linear chain enough mobility and nucleation capability became the determining factor. Based on the perfect nucleation capability of star-shaped chain, the crystallization rate of 4sPLLA/4sPDLA ranked first, followed by those of 4sPLLA/PDLA and PLLA/4sPDLA. Lack of enough nuclei, linear PLLA/PDLA showed little crystallization peak.

In Fig. 7(d), crystallinity of star-shaped and linear scPLAs after complete isothermal crystallization was plotted versus temperature. As we can see, structure and temperature had a large effect on the crystallinity of scPLAs. Linear PLLA/PDLA reduced its crystallinity when temperature increased from 120 °C to 140 °C, while 4sPLLA/PDLA and PLLA/4sPDLA experienced an opposite tendency. For 4sPLLA/4sPDLA, the crystallinity first increased from 120 °C to 130 °C, followed by a decrease from 130 °C to 140 °C. The complicated result was probably caused by the synthetic role of nucleation, growth and integrity restriction of crystals. In other words, the crystallinity was a function of structure of scPLAs and temperature. It is observed that linear chains could lead to higher crystallinity than branched ones for PLAs because of fewer defects occurring on crystals interface, so did scPLAs. More perfect crystals and good crystallization process offered linear PLLA/PDLA the highest crystallinity at 120 °C. With temperature increasing, worse crystallization process presented in Figs. 7(b) and 7(c) made its crystallinity on the decrease. Owing to the restriction of star-shaped chains, 4sPLLA/4sPDLA almost revealed the lowest crystallinity with defective crystals although it kept a fairly rapid crystallization rate in Figs. 7(a) –7(c). It should be noted that at 140 °C 4sPLLA/4sPDLA had a higher crystallinity than PLLA/PDLA since higher temperature promoted the perfect extent of crystals and 4sPLLA/4sPDLA crystallized better. As for 4sPLLA/PDLA and PLLA/4sPDLA, the mixture of linear chain and star-shaped chain combined the advantage of excellent crystallization behavior and perfect crystals morphology, resulting in the highest crystallinity.

To better show the isothermal crystallization kinetics, the relative degree of crystallinity, X_t, regarded as a function of time is presented in Fig. 8. X_t is calculated as follows[16]:

$$X_t = \frac{1}{\Delta H_c} \times \int_0^t \left(\frac{dH}{dt} \right) dt \tag{3}$$

where dH/dt is the heat release rate, and ΔH_c is the total heat, *i.e.* the total peak area in Figs. 8(a)–8(c). Typical sigmoidal evolution curve was demonstrated with an induction period and a rapid growth period. As seen from Figs. 8(a)–8(c), all of the scPLAs needed more time when T_{iso} increased from 120 °C to 140 °C because of fewer nuclei and more time to develop crystals with less defects. In addition, crystallization induction time of linear PLLA/PDLA was longer than that of star-shaped sc samples due to its worse nucleation ability, especially at higher temperature. As temperature increased, the sigmoidal evolution of 4sPLLA/4sPDLA shifted from nearly the longest time in Fig. 8(a) to the shortest time in Fig. 8(c) relative to the other three scPLAs, suggesting the change of crystallization stability with temperature.

The crystallization half-time, $t_{1/2}$, an essential index to characterize the crystallization kinetics, was obtained from the relative crystallinity curve versus time in Figs. 8(a)–8(c). It is defined as the time required to reach X_t = 50% and shown in Fig. 8(d) against isothermal temperature. All of the scPLAs displayed a continuously upward tendency with increase in temperature. A sharp rise of $t_{1/2}$ appeared on PLLA/PDLA from 1.5 min to 14 min, while 4sPLLA/4sPDLA presented a slowest increase from 1.4 min to 2.4 min, conforming the speculation that star-shaped chain would increase the crystallization rate of scPLA.

Avrami equation is usually applied to study the isothermal crystallization kinetics as follows[33]:

$$X_t = 1 - \exp\left(-kt^n\right) \tag{4}$$

where X_t is the relative degree of crystallinity described in Eq. (3), n is the Avrami index and k is the overall rate constant. Eq. (4) can also be described in the linear form:

$$\ln[-\ln(1 - X_t)] = n\ln t + \ln k \tag{5}$$

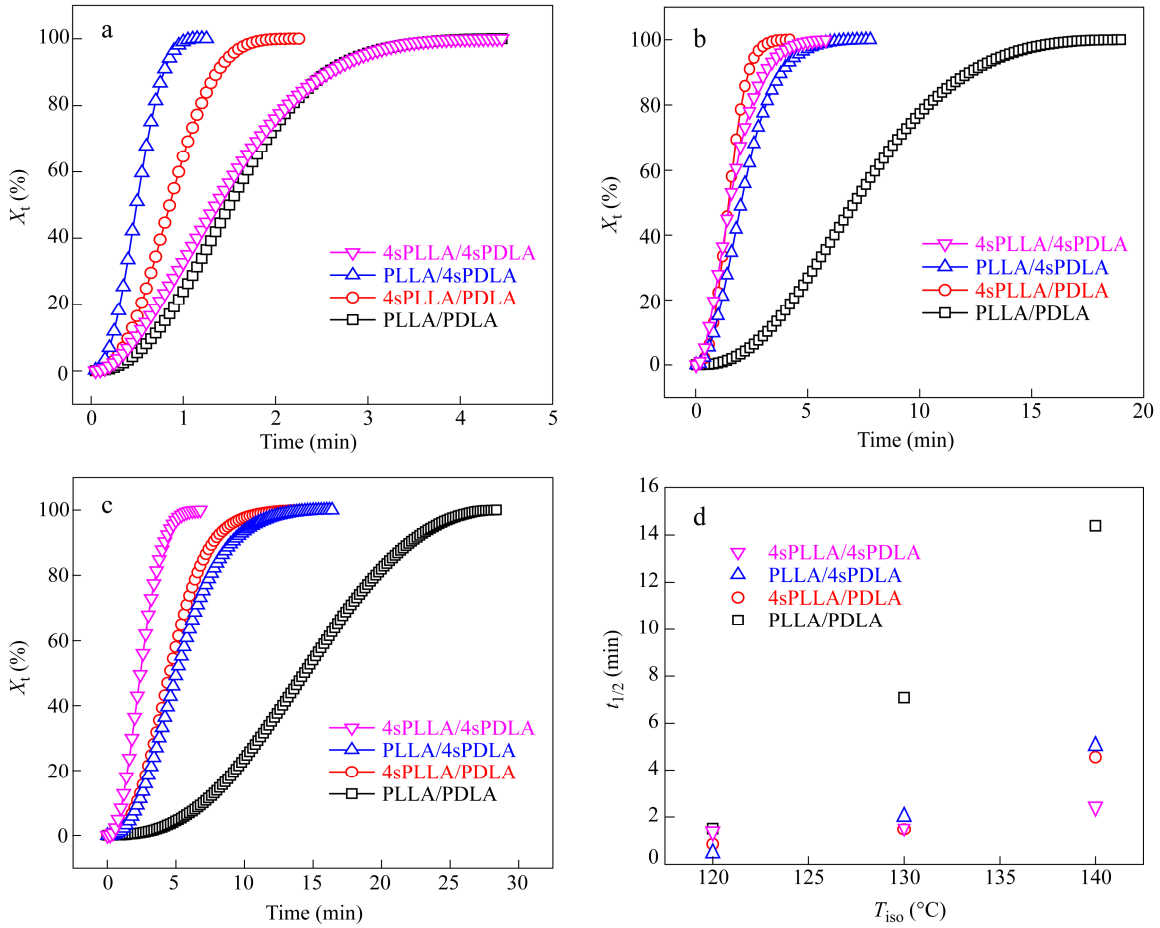


Fig. 8 Relative crystallinity as a function of time for sc specimen after isothermal crystallization at (a) 120 °C, (b) 130 °C and (c) 140 °C; (d) Crystallization half-time achieved at these temperatures

By linear fitting of ln[−ln(1 − X_t)] versus ln$t$, n and ln$k$ are obtained as the slope and intercept in Fig. 9, respectively. In order to ensure the accuracy of n and k, data of X_t between 5% and 20% in Fig. 8 were employed. The data of Avrami constant are shown in Table 2. Avrami index n depends on mechanism of nucleation and growth pattern. n for PLLA/PDLA, 4sPLLA/PDLA, PLLA/4sPDLA ranged between 2 and 3, and for 4sPLLA/4sPDLA was below 2 at 120 °C, indicating that heterogeneous nucleation and star-shaped chain would make crystals develop toward more irregular spherulites below 130 °C. At 140 °C, restriction of star-shaped chain was loosened and spherulites became more perfect for 4sPLLA/4sPDLA. Besides, the data rate constant k displayed the advantage of star-shaped chain in crystallization rate, consistent with the result of $t_{1/2}$ in Fig. 8(d) at higher temperature.

In order to confirm the previously mentioned effect of chain architecture on scPLA crystallization, isothermal crystallization behaviors of sc samples were observed by polarized optical microscope. Similar to the above measurement, sc samples were first melted at 260 °C for 3 min to destroy the thermal history, then cooled

to required temperature with the fastest speed. Micrographs were obtained by taking photographs at an appropriate time interval. The selected micrographs at isothermal crystallization temperature of 140, 130 and 120 °C are presented in Fig. 10 and spherulite density calculated from the micrographs is presented in Fig. 11.

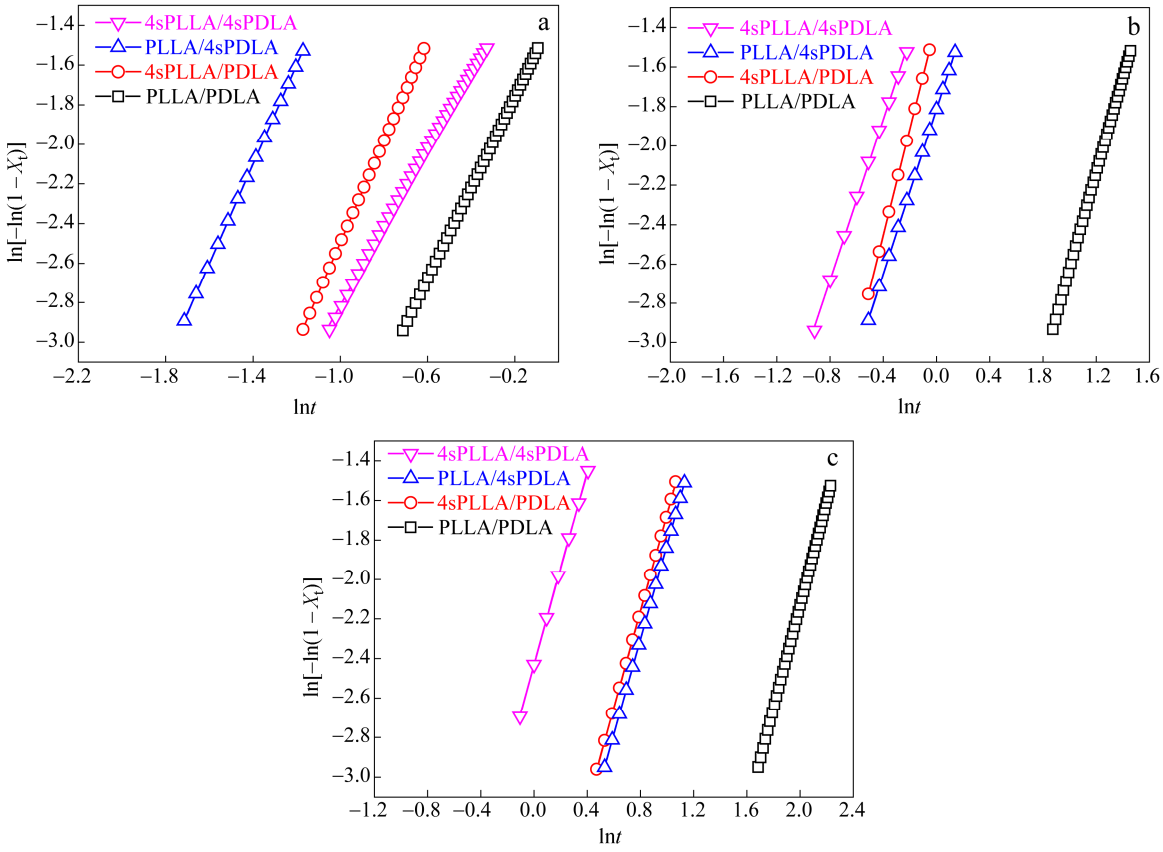


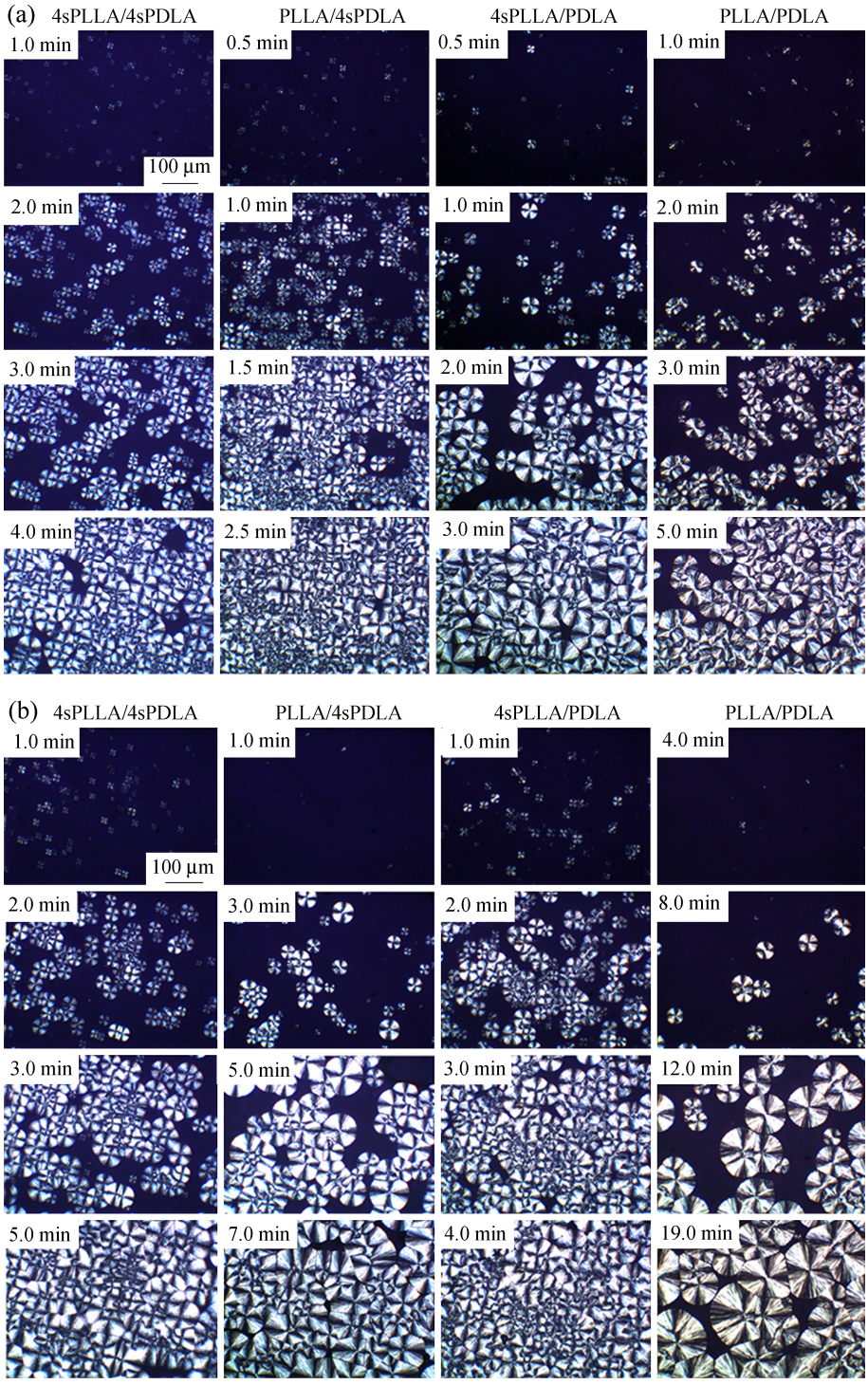
Fig. 9 Avrami plots for sc specimen after isothermal crystallization at (a) 120 °C, (b) 130 °C and (c) 140 °C

Table 2 Kinetic parameters obtained from Avrami model

Sample	120 °C		130 °C		140 °C	
	n	k	n	k	n	k
4sPLLA/4sPDLA	1.963	0.427	2.039	0.350	2.437	0.088
PLLA/4sPDLA	2.509	4.103	2.090	0.163	2.396	0.015
4sPLLA/PDLA	2.556	1.062	2.700	0.253	2.449	0.016
PLLA/PDLA	2.302	0.273	2.425	0.006	2.612	0.001

All of the four sc samples exhibited typical cross extinction pattern of spherulite and spherulite grew with increase in time until screen was covered with crystals. Obviously, isothermal crystallization temperature and chain structure both had an effect on the completion time of crystallization. At 120 °C, the crystallization time ranged from 2.5 min for PLLA/4sPDLA to 5 min for PLLA/PDLA. When isothermal crystallization temperature grew to 130 °C, crystallization time increased and ranged from 4 min for 4sPLLA/PDLA to 19 min for PLLA/PDLA. A larger difference occurred when 6 min and 30 min were spent for the fastest crystallization of 4sPLLA/4sPDLA and slowest crystallization of PLLA/PDLA. Consistent with the isothermal DSC test results, the phenomenon could be accounted by the nucleation capability and growth ability of scPLAs with different chain structure. As shown in Fig. 11, on one hand, nucleation capability reduced with isothermal crystallization temperature increase, on the other hand, 4sPLLA/4sPDLA had the most crystals while PLLA/PDLA had the least amount of crystals, proving the acceleration effect of star-shaped chain on nucleation. In addition, with the

rise of temperature, all of the sc samples presented more perfect spherulites. It should be noted that linear PLLA/PDLA exhibited more beautiful and perfect spherulites than star-shaped sc at similar conditions, demonstrating linear chain was more beneficial to the growth of crystals and the increase of the crystallinity from one aspect.



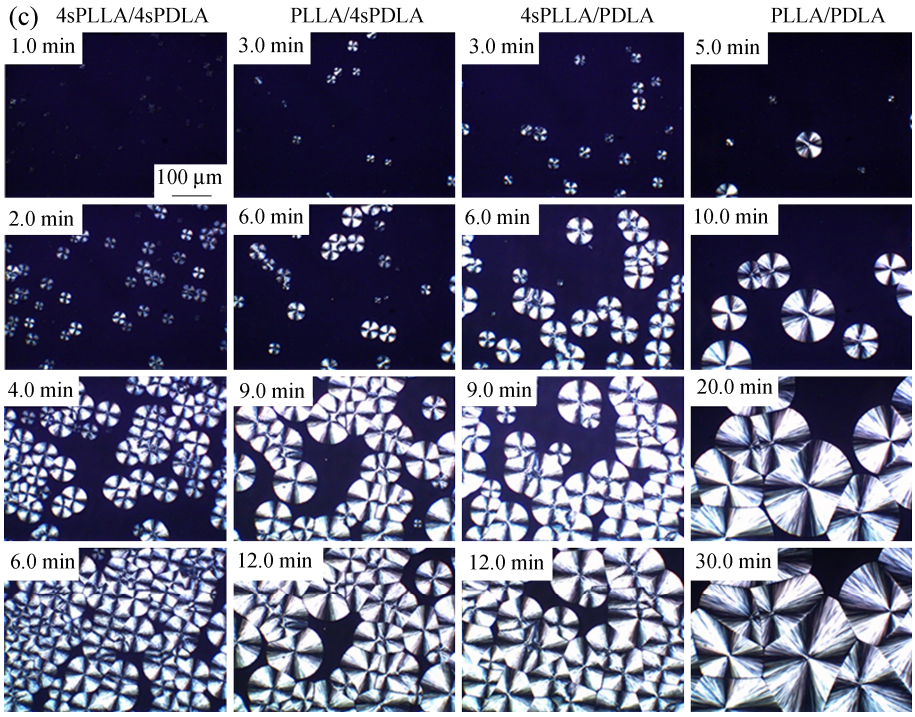


Fig. 10 POM images during isothermal crystallization for 4sPLLA/4sPDLA, PLLA/4sPDLA, 4sPLLA/PDLA and PLLA/PDLA at (a) 120 °C, (b) 130 °C and (c) 140 °C (All the scale bars are the same.)

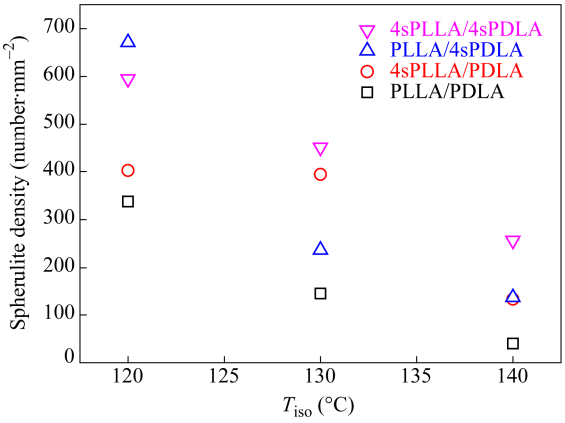


Fig. 11 Spherulite density as a function of temperature for sc specimen observed from POM images during isothermal crystallization

Spherulite radius versus time by measurement of crystals size of POM photographs for sc specimen at 120, 130 and 140 °C in Fig. 9 is demonstrated in Figs. 12(a)–12(c). Due to the approximate linear growth relationship between spherulite radius and time, spherulite radius growth rate was obtained by linear fitting of spherulite radius versus time as the slope and presented in Fig. 12(d). The radius growth rate of the sc samples first increased as isothermal crystallization temperature increased from 120 °C to 130 °C, followed by a dramatic decrease when temperature was continuously increased to 140 °C. What is more, 4sPLLA/PDLA and PLLA/4sPDLA ranked first in growth rate, and linear PLLA/PDLA the last at 120 and 130 °C, which changed when 4sPLLA/4sPDLA grew the fastest at 140 °C. The distinction of radius growth tendency with different structure might be caused by the complicated combined action of chain mobility and secondary nucleation with temperature change.

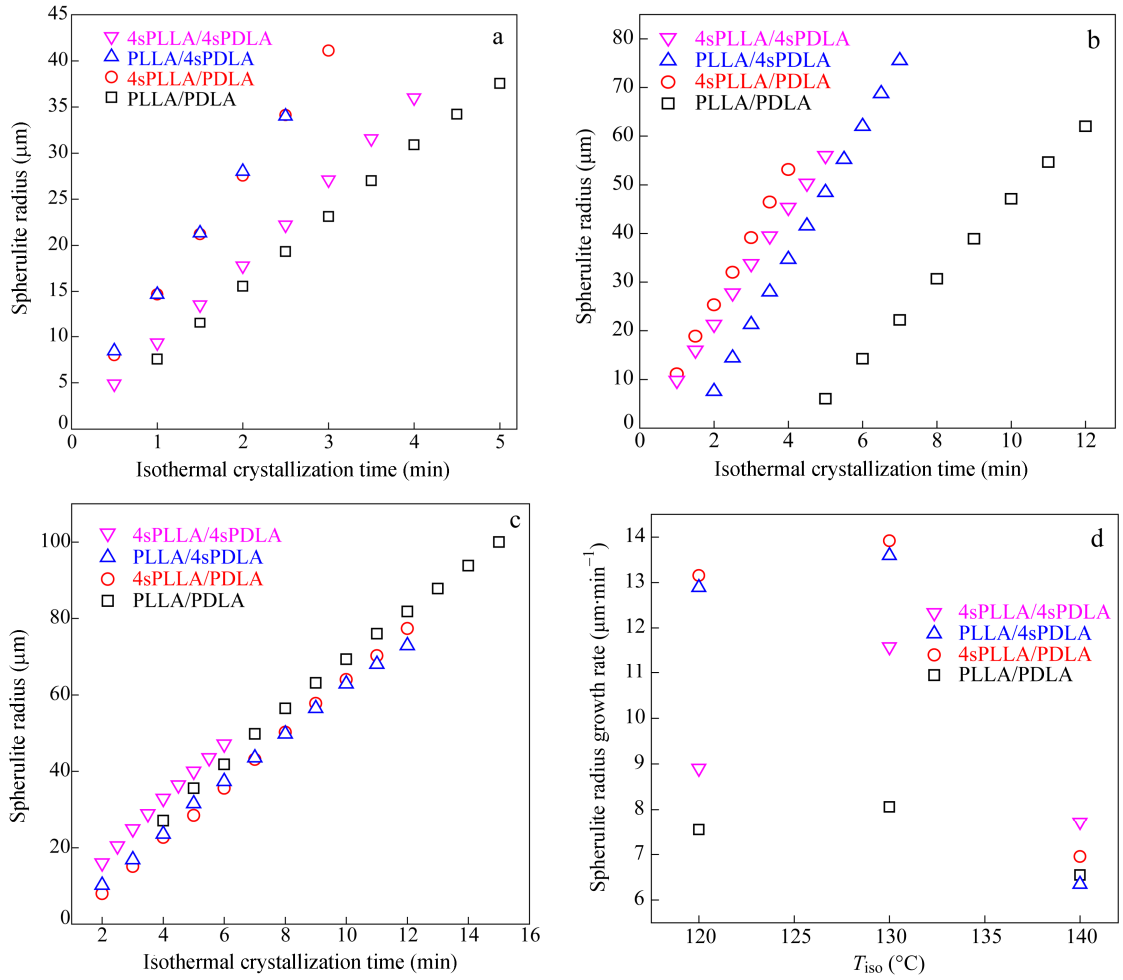


Fig. 12 Spherulite radius plot versus time during isothermal crystallization for 4sPLLA/4sPDLA, PLLA/4sPDLA, 4sPLLA/PDLA and PLLA/PDLA at (a) 120 °C, (b) 130 °C, (c) 140 °C; (d) Spherulite radius growth rate obtained at these temperatures

CONCLUSIONS

In this work, four kinds of scPLAs with various chain architectures were prepared by solution blending of PLLAs and PDLAs. ^{1}H-NMR, FTIR and WAXD tests confirmed the successful and perfect formation of PLA stereocomplexes. The non-isothermal and isothermal crystallization behaviors of scPLAs were investigated to reveal the effect of chain structure on crystallization of scPLAs. Crystallization of 4sPLLA/PDLA and PLLA/4sPDLA was enhanced as evidenced by faster crystallization, higher crystallinity and no cold crystallization compared with PLLA/PDLA and 4sPLLA/4sPDLA due to the increased spherulite density of star-shaped chain, which can be proved by POM photographs and good chain mobility of linear chain in dynamic test. Isothermal DSC test verified the advantage of star-shaped structure in crystallization kinetics as $t_{1/2}$ of 4sPLLA/4sPDLA had the minimum increase while PLLA/PDLA increased largest as a result of the better nucleation capacity of star-shaped architecture presented in isothermal POM photographs. Meanwhile, 4sPLLA/PDLA and PLLA/4sPDLA behaved best in crystallinity in relation to PLLA/PDLA with limitation in nucleation capacity at higher temperature and 4sPLLA/4sPDLA with restriction in star-shaped chain as evidenced by the fewest crystals for PLLA/PDLA and the imperfect spherulite for 4sPLLA/4sPDLA appeared in isothermal POM photographs. The abnormal Avrami exponent of 4sPLLA/4sPDLA at 120 and 130 °C also

suggested that change of crystal growth mechanism was affected by two kinds of star-shaped chain at lower temperature. Combining the above analyses, we drew a conclusion that the mixture of star-shaped and linear chain or two kinds of star-shaped chain would promote the crystallization of PLA stereocomplex at higher temperature.

REFERENCES

1 Zhao, L.F., Cheng, J., Tian, X.J. and Zhang, R.L., Chinese J. Polym. Sci., 2015, 33(3): 499
2 Solarski, S., Mahjoubi, F., Ferreira, M., Devaux, E., Bachelet, P. and Bourbigot, S., J. Mater. Sci., 2007, 42(13): 5108
3 Xiang, S., Jun, S., Li, G., Bian, X.C., Feng, L.D., Chen, X.S., Liu, F.Q. and Huang, S.Y., Chinese J. Polym. Sci., 2016, 34(1): 69
4 Oh, J.K., Soft Matter, 2011, 7(11): 5100
5 Lasprilla, A.J.R., Martinez, G.A.R., Lunelli, B.H., Jardini, A.L. and Maciel Filho, R., Biotechnol. Adv., 2012, 30(1): 323
6 Saeidlou, S., Huneault, M.A., Li, H. and Park, C.B., Prog. Polym. Sci., 2012, 37(12): 1659
7 Li, Y., Wang, Y., Liu, L., Han, L., Xiang, F. and Zhou, Z., J. Polym. Sci., Part B: Polym. Phys., 2009, 47(3): 328
8 Hashima, K., Nishitsuji, S. and Inoue, T., Polymer, 2010, 51(17): 3935
9 Lim, L.T., Auras, R. and Rubino, M., Prog. Polym. Sci., 2008, 33(8): 824
10 Na, B., Tian, N., Lv, R., Zou, S., Xu, W. and Fu, Q., Macromolecules, 2010, 2(43): 1156
11 Harris, A.M. and Lee, E.C., J. Appl. Polym. Sci., 2008, 107(4): 2248
12 Schmidt, S.C. and Hillmyer, M.A., J. Polym. Sci., Part B: Polym. Phys., 2001, 39(3): 302
13 Tsuji, H., Takai, H., Fukuda, N. and Takikawa, H., Macromol. Mater. Eng., 2006, 291(4): 325
14 Fehri, S., Cinelli, P., Coltelli, M.B., Anguillesi, I. and Lazzeri, A., Int. J. Chem. Eng. Appl., 2016, 7(2): 85
15 Zhang, Y., Chinese J. Polym. Sci., 2013, 31(9): 1276
16 Yin, H.Y., Wei, X.F., Bao, R.Y., Dong, Q.X., Liu, Z.Y., Yang, W., Xie, B.H. and Yang, M.B., CrystEngComm, 2015, 17(23): 4334
17 Pillin, I., Montrelay, N. and Grohens, Y., Polymer, 2006, 47(13): 4676
18 Xiao, H., Lu, W. and Yeh, J.T., J. Appl. Polym. Sci., 2009, 113(1): 112
19 Kulinski, Z. and Piorkowska, E., Polymer, 2005, 46(23): 10290
20 Zhou, J., Jiang, Z., Wang, Z., Zhang, J., Li, J., Li, Y., Zhang, J., Chen, P. and Gu, Q., RSC Adv., 2013, 3(40): 18464
21 Pan, P., Liang, Z., Zhu, B., Dong, T. and Inoue, Y., Macromolecules, 2009, 42(9): 3375
22 Yang, S., Wu, Z.H., Yang, W. and Yang, M.B., Polym. Test., 2008, 27(8): 958
23 Ikada, Y., Jamshidi, K., Tsuji, H. and Hyon, S.H., Macromolecules, 1987, 20(4): 904
24 Okihara, T., Tsuji, M., Kawaguchi, A., Katayama, K.I., Tsuji, H., Hyon, S.H. and Ikada, Y., J. Macromol. Sci., Part B: Phys., 1991, 30(1-2): 119
25 Zhang, J., Sato, H., Tsuji, H., Noda, I. and Ozaki, Y., Macromolecules, 2005, 38(5): 1822
26 Fan, Y., Nishida, H., Shirai, Y., Tokiwa, Y. and Endo, T., Polym. Degrad. Stab., 2004, 86(2): 197
27 Regnell Andersson, S., Hakkarainen, M., Inkinen, S., Södergård, A. and Albertsson, A.C., Biomacromolecules, 2012, 13(4): 1212
28 Tsuji, H., Macromol. Biosci., 2005, 5(7): 569
29 Cheerarot, O. and Baimark, Y., J. Chem., 2015, DOI: 10.1155/2015/206123
30 Wang, Y. and Mano, J.F., J. Appl. Polym. Sci., 2008, 107(3): 1621
31 Brochu, S., Prud'Homme, R.E., Barakat, I. and Jerome, R., Macromolecules, 1995, 28(15): 5230
32 Furuhashi, Y., Kimura, Y., Yoshie, N. and Yamane, H., Polymer, 2006, 47(16): 5965
33 Tsuji, H., Adv. Drug. Del. Rev., 2016, 107: 97
34 Inkinen, S., Stolt, M. and Södergård, A., Polym. Adv. Technol., 2011, 22(12): 1658
35 Shao, J., Sun, J., Bian, X., Cui, Y., Li, G. and Chen, X., J. Phys. Chem. B., 2012, 116(33): 9983
36 Biela, T., Duda, A. and Penczek, S., Macromolecules, 2006, 39(11): 3710

37 Nouri, S., Dubois, C. and Lafleur, P.G., Polymer, 2015, 67: 228
38 Tan, B.H., Hussain, H., Lin, T.T., Chua, Y.C., Leong, Y.W., Tjiu, W.W., Wong, P.K. and He, C.B., Langmuir, 2011, 27(17): 10538
39 Purnama, P., Jung, Y. and Kim, S.H., Polym. Degrad. Stab., 2013, 98(5): 1097
40 Gardella, L., Basso, A., Prato, M. and Monticelli, O., RSC Adv., 2015, 5(58): 46774
41 Sakamoto, Y. and Tsuji, H., Macromol. Chem. Phys., 2013, 214(7): 776
42 Geschwind, J., Rathi, S., Tonhauser, C., Schömer, M., Hsu, S.L., Coughlin, E.B. and Frey, H., Macromol. Chem. Phys., 2013, 214(13): 1434
43 Nagahama, K., Nishimura, Y., Ohya, Y. and Ouchi, T., Polymer, 2007, 48(9): 2649
44 Nagahama, K., Fujiura, K., Enami, S., Ouchi, T. and Ohya, Y., J. Polym. Sci., Part A: Polym. Chem., 2008, 46(18): 6317
45 Nederberg, F., Appel, E., Tan, J.P.K., Kim, S.H., Fukushima, K., Sly, J. and Hedrick, J.L., Biomacromolecules, 2009, 10(6): 1460
46 Shao, J., Tang, Z., Sun, J., Li, G. and Chen, X., J. Polym. Sci., Part B: Polym. Phys., 2014, 52(23): 1560
47 Tsuji, H., Matsumura, N. and Arakawa, Y., J. Phys. Chem. B., 2016, 120(6): 1183
48 Tsuji, H. and Tajima, T., Macromol. Mater. Eng., 2014, 299(9): 1089
49 Bao, J., Han, L., Shan, G., Bao, Y. and Pan, P., J. Phys. Chem. B., 2015, 119(39): 12689
50 Long, L., Zhao, J., Li, K., He, L., Qian, X., Liu, C., Wang, L., Yang, X., Sun, J., Ren, Y., Kang, C. and Yuan, X., Mater. Chem. Phys., 2016, 180: 184
51 Fischer, E.W., Sterzel, H.J. and Wegner, G., Colloid. Polym. Sci., 1973, 251(11): 980
52 Tsuji, H., Horii, F., Nakagawa, M., Ikada, Y., Odani, H. and Kitamaru, R., Macromolecules, 1992, 25(16): 4114
53 Routaray, A., Mantri, S., Nath, N., Sutar, A.K. and Maharana, T., Chinese Chem. Lett., 2016, 27(12): 1763
54 Na, B., Zou, S. and Lv, R., J. Macromol. Sci., Part B: Phys., 2014, 53(1): 162